International Journal of Computational and Experimental Science and ENgineering (IJCESEN)

Vol. 11-No.4 (2025) pp. 9560-9568

http://www.ijcesen.com

ISSN: 2149-9144

Research Article

Calculation of pressure and velocity vector field in a porous medium

Azzazen Mohamed[1]*, Medkour Mihoub[2]

[1]Aeronautics and Space Studies Institute, Aeronautical Sciences Laboratory, University of Saad Dahlab -Blida I-, 09000, Algeria

* **Corresponding Author Email:** m.azzaen@gmail.com - **ORCID:** 0009-0004-4533-0721

[2]Medkour Mihoub, University Tissemselt ,38000 , Algérie

Email: medkour.mihoub@univ-Tissemsilt.dz - **ORCID:** 0009-0004-4533-0981

Article Info:

DOI: 10.22399/ijcesen.4475
Received: 07 July 2025
Revised: 20 November 2025
Accepted: 30 November 2025

Keywords

reservoir engineering
Navier Stocks3 equation
Darcy's law
Peng-Robinson equation
Single-phase flow

Abstract:

The most notable omission, among the topics addressed in reservoir engineering, is the absence of any serious discussion on the complexities of hydrocarbon phase behavior. For this reason, we have tried to address this subject with great precision and care, which can be summarized in the process of illustrating the main functions of a reservoir engineer, namely estimating the hydrocarbons in place, calculating a recovery factor, and attaching a timescale to the recovery. This article presents many fundamental concepts of reservoir engineering.In our porous medium, which is a real gas deposit, we assumed that the temperature is constant at 170 F° and that the pressure varies between 2600 (psia) and 2000 (psia) in order to determine the behavior of a gas reservoir and to better understand the phase transformations (single-phase to two-phase) for the ideal extraction of the latter. The molar mass of this gas is considered constant $M = 18,82\ (g/mol)$, the density is $\rho = 4.31(g/l)$.Let us consider a simple simulation in which our tank contains the gas with these different elements and is subjected to a constant temperature and a continuously increasing pressure. At a specific pressure (the critical pressure), during this study, the gas, which was entirely in a liquid phase at high pressure, evaporates. For this reason, it was necessary to maintain the pressure in the tank at a value of 2600 (psia) to ensure significant gas extraction, as demonstrated in our study.The application of the Peng-Robinson equation is the most important for reservoir gas because it will give us very important results compared to the ideal gas equation and it is described in several works that deal with the same subject.

1. Introduction

The important aspect in the study of flow in a porous medium is the nature of the fluids in the pores, which determines the mathematical formulas of the model used to describe mechanical and thermodynamic phenomena related to the flow. The simplest case is single-phase flow, where porous media are completely filled with single-phase fluid. Single-phase flows in porous media appear to be of great interest in several situations to science and applied technology. For example, in some recently discovered oil or gas reservoirs, which are in the exploration phase, the flow is essentially single-phase [1-5], In reservoir engineering, the most important and useful thing is production, and especially pressure, which is directly or indirectly linked in all phases of reservoir studies. It is used to characterize the physical state (liquid or gas or both) of a reservoir, calculate the reserves in place and predict the future behavior of the reservoir, therefore forecasting with the results of numerical simulations, so porous media are of great interest to the oil industry and from these results it is possible to understand certain aspects of the flow, consequently, to determine the best regimes and exploration techniques [6-11],

The study, presented in this paper, falls within the framework of gas reservoir engineering. Our goal is to determine the pressure distribution and predict the behavior of these reservoirs and then calculate the production summarized in the extraction well term in the mass conservation equations, under the various injection and production conditions, using the numerical simulation presented with a program in fortran 90 where we inject real values reported from an oil zone among the 25 zones of Hassi - Messaaoud, which is zone 15 [12-17].

1- Pressure-Temperature Diagram

Figure -1- presents a typical pressure-temperature diagram for a three-phase system and using this diagram we will determine the behavior of this tank starting from a pressure of 2600 (psia) and a temperature of (160 F^0) down to 1500 (psia) and (160 F^0)

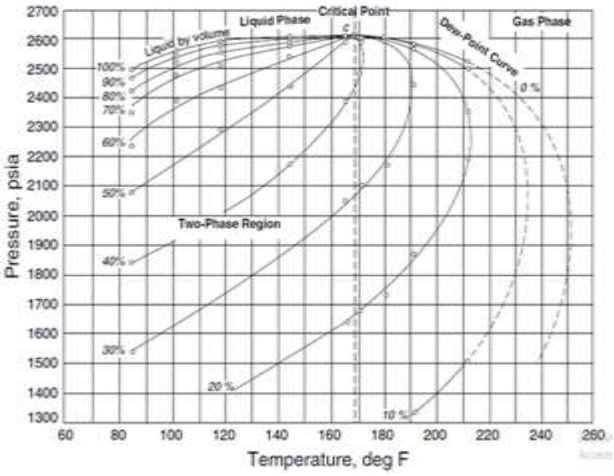

Figure 1. *Typical P-T diagram for a three-phase system.*

2. Mathematical Model

2.1 Domain Configuration

The modeling of flow in a porous medium relies on a number of simplifying assumptions. In this work, we consider the geometry of the porous medium to be essentially three-dimensional, with a thickness H and horizontal dimensions Lx, Ly, and Ly.

The area under study comprises five wells: one injector well in the middle and four production wells, arranged in a rectangular geometry shown in Figure 2 below.

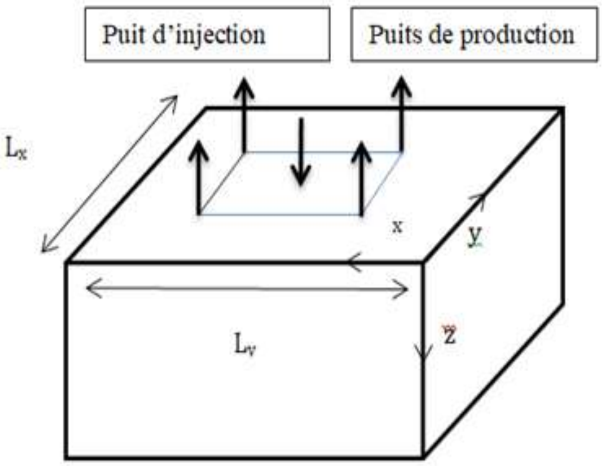

Figure 2. *The geometry of the porous medium.*

2.2 Assumptions

Consider a single-phase, liquid-like gas flow, slightly compressible, in a homogeneous porous medium. The injection of gas (CO2) into the reservoir is assumed to behave like an insoluble gas. This condition allows for an efficient increase in pressure within the reservoir.

Capillary effects are neglected in this model.

Under the following assumptions, we obtain a simplified form of the system of equations to be solved:

- The compressibility of fluid □□ is low.
- The porosity of the medium is constant.
- The permeability is also assumed to be constant.
- The density and viscosity vary with pressure, creating nonlinearities in our system.

2.3 Governing Equations

To establish the equations describing the single-phase flow of a fluid in a porous medium, it is necessary to rely on several fundamental laws, including:

- The law of conservation of mass
- Darcy's law
- The equations of state of fluids

2.3.1 Mass Conservation Equation

The mass conservation equation, or continuity equation, for a fluid in a porous medium, is written in the following differential form:

$$-\left(\frac{\partial(\rho u_x)}{\partial x}+\frac{\partial(\rho u_y)}{\partial y}+\frac{\partial(\rho u_z)}{\partial z}\right)=\frac{\partial \rho\phi}{\partial t}+\bar{q} \qquad (1)$$

2.3.2 Darcy's Equation

For modeling flows in more complex media (such as heterogeneous media or those involving compressible fluids), a generalized form of Darcy's law is used, expressed in Cartesian coordinates (x,y,z), in differential form:

$$\overrightarrow{u_x}=-\frac{k}{\mu}\left(\frac{\partial p}{\partial x}\right) \qquad (2)$$

$$\overrightarrow{u_y}=-\frac{k}{\mu}\left(\frac{\partial p}{\partial y}\right) \qquad (3)$$

$$\overrightarrow{u_z}=-\frac{k}{\mu}\left(\frac{\partial p}{\partial z}\right) \qquad (4)$$

where:

$\vec{u}$ is the Darcy velocity vector,

k is the permeability of the medium,

μ is the dynamic viscosity of the fluid,

∇P is the pressure gradient.

2.3.3 Equations governing the model:

$$\begin{cases} \dfrac{\partial(\rho\phi)}{\partial t} + \nabla(\rho u) = q \\ u = -\dfrac{k}{\mu}\nabla P \\ P(x,y,0) = P_0 \forall x \in \Omega \end{cases} \tag{5}$$

The correlation between density and viscosity, which introduces non-linearities into the system (equation 5), will be modeled using the Peng-Robinson equation of state, in order to simplify the treatment of the derivatives of these quantities.

2.4 Thermodynamic Model for Density:

2.4.1 The Peng-Robinson Cubic Equations of State:

In 1976, Peng and Robinson proposed an improved form for the attractive term to better model the saturated volumetric properties of hydrocarbons. Although this equation remains imperfect near the critical point, notably due to an overestimation of □□, it is widely used to represent petroleum fluids. It generally gives satisfactory results. This equation of state can be expressed as a cubic polynomial, used to calculate the density of a fluid as a function of its pressure and temperature:

$$v^3 - \left(\frac{RT}{P} - b\right)v^2 + \left(\frac{a}{P} - \frac{2bRT}{P} - 3b^2\right)v - b\left(\frac{a}{P} - \frac{bRT}{P} - b^2\right) = 0 \tag{6}$$

The repulsion (b) and attraction (a) parameters are obtained either from critical properties or by fitting experimental data. They are defined by:

$$b = 0,077796\frac{RT_c}{P_c} \tag{7}$$

$$a = a_c\alpha \tag{8}$$

$$a_c = 0.457235\frac{(RT_c)^2}{P_c} \tag{9}$$

The factor α, proposed by Peng and Robinson, adopts the form introduced by Soave. It depends on the acentric factor   via the parameter *m*:

$$m = 0,37464 + 1,54226w - 0,26992w^2 \tag{10}$$

Therefore, the function α can be expressed as:

$$\alpha = \left[1 + m\left(1 - \sqrt{\frac{T}{T_C}}\right)\right]^2 \tag{11}$$

2.4.2 Extension of the Peng-Robinson Equation to Mixtures

The equations of state developed for pure substances can be adapted to mixtures by taking into account the interactions between the different constituents, using mixing rules that modify the parameters of the equation to reflect the overall behavior of the system. The first form of mixing rule is that of Vander Waals, known as the "Classical Mixing Rule," which gives the following expressions for the mixing repulsion and attraction parameters.

$$a_m = \sum_i x_i a_i = a_{mc}\alpha_m \tag{12}$$

$$b_m = \sum_i x_i b_i = 0..077796\frac{RT_{mc}}{P_{mc}} \tag{13}$$

With: x_i mole fraction for constituents (i).

Where, a_i and b_i represent the repulsion and attraction parameters corresponding to constituent (i), Tmc is the critical mixing temperature, P_{mc} is the critical mixing pressure, a_{mc} is the critical mixing repulsion parameter, and αm is the constant alpha for the mixture [18-24].

2.4.3 The HASSI – MESSAOUD gas (HMD)

In the petroleum context, when we talk about the constituents of gas in deposits in porous media, we are referring to the typical composition of natural gases present in underground reservoirs (deposits), which are trapped in porous media such as sedimentary rocks (sandstone, limestone, shale, etc.).

The gas found in the Hassi-Messaoud field is very light. Under the temperature and pressure conditions of the reservoir,

Table 1. presents the mass percentages measured at a site located south of the Industrial Control Center (SIC) [25-30].

Table 1. *Actual composition of each constituent of the gas in the HASSI – MESSAOUD field.*

CO_2	8.5802	**n-c8**	0.1557
Nitrogen	0.5255	**n-c7**	0.3212
Methane	81.3798	**n-c9**	0.2323
Ethane	5.0603	**n-c10**	0.1429
Propane	1.8813	**n-c11**	0.0493
i-butane	0.5896	**n-c12**	0.0270
n-butane	0.5804	**H2o**	0.0101

The critical coordinates which allow the application of the PENG and ROBINSON equation are shown in Table 2. [20].

Table 2.*Critical parameters of pure substances (ARTEP database [20])*

composition de gaz	Temperature critique	Presion critique	Facteur acentriqu

	(K)	(MPa)	e w
Nitrogen	678.0	1.74	0.618
CO_2	190.6	4.596	0.012
Methane	305.2	4.8839	0.099
Ethane	369.75	4.25	0.152
Propane	425.15	3.796	0.200
i-butane	470.35	3.347	0.252
n-butane	507.4	2.97	0.296
H2o	678.0	1.74	0.618
n-c7	540.5	2.74	0.351
n-c8	570.4	2.51	0.396
n-c9	596.8	2.31	0.441
n-c10	620.2	2.14	0.486
n-c11	641.4	1.99	0.530
n-c12	660.6	1.85	0.575

According to the definition of mole fraction, we have:

$$x_i = \frac{n_i}{n_T} = \frac{n_i}{\sum_{j=1}^{n} n_j} \tag{14}$$

Or:

n_T :Total number of moles of constituent i.

And the number of moles in (g)

$$n = \frac{m}{M} \tag{15}$$

m: mass of the constituent in (g).

M: molar mass of the compound in ($g.mol^{-1}$).

The critical properties (and possibly its acentric factor) are then determined from those of the pure constituents, by applying empirical weighting rules. The simplest weighting rule (KAY, 1936) is linear [18].

$$P_c = \sum_{i=1}^{n} x_i P_{ci} \tag{16}$$

P_{ci} : The critical pressure of constituents i.

$$T_c = \sum_{i=1}^{n} x_i T_{ci} \tag{17}$$

T_{ci} : The critical temperature of constituents i.

The acentric factor is calculated using the pseudo-critical coordinates rule.

$$w = \sum_{i=1}^{n} x_i w_i \tag{18}$$

w_i : The acentric factor of constituent i.

x_i ; Mole fraction of constituent i.

Table 3. *Application of the three equations (16) and (17) and (18)*

gas composition	$X_i P_{ci}$	$X_i T_{ci}$	$X_i w_i$
Nitrogen	0.248	10.086	0.001
Co2	0.114	8.371	0.002
Méthane	0.043	3.767	0.002
Ethane	0.026	2.920	0.001
Propane	0.034	4.767	0.003
i-butane	0.010	1.645	0.001
n-butane	0.010	1.884	0.001
H2o	0.029	6.603	0.005
n-c7	0.027	7.082	0.005
n-c8	0.032	9.136	0.007
n-c9	0.122	39.315	0.032
n-c10	0.690	246.455	0.215
n-c11	0.004	1.743	0.002
n-c12	0.003	1.135	0.001

Therefore, the pressure, temperature, and acentric factor are Pc = 2.051 MPa, Tc = 661.714 K^0, w=0.597.

Critical compressibility factor Zc

To calculate the value of Zc, we use the Nath method, which is simpler and more recent than other methods. Zc = 0.2918 - 0.0928W, we will have Zc = 0.236 with critical molar volume Vc

We have $Z_c = \frac{PV_c}{RT_c}$ then $V_c = \frac{RT_c}{PZ_c}$ therefore

$V_c = 36259.018\left(cmg^3 / g\ mol\right)$

The molar mass of this gas is determined according to the following expression [21].

$$M = \sum_{i=1}^{n} x_i M_i \tag{19}$$

M_i: The molar mass of component i in (g/mol).

The molar mass will be equal to M=211.939(g/mol).

Correlations for viscosity

For the calculation of viscosity, we use the correlation proposed by Jossi, Stiel, and Thodos, expressed by the following equation:

$$\begin{aligned}[(\mu-\mu^*)\zeta+1]^{1/4} &= 1.0230+0.233\rho_r \\ &+0.58533\rho_r^{\,2}-0.40758\rho_r^{\,3}+0.093324\rho_r^{\,4}\end{aligned} \tag{20}$$

It is important to note that: $\rho_r = \frac{\rho}{\rho_c} = \frac{v_c}{v}$ Where the volume n here is calculated beforehand by the Peng – Robinson equation, $\xi = T^{-1/6} M^{1/2} P^{2/3}$, μ^* is the value of the viscosity at low pressure, calculated by the following formulations [31].

When T < 1.5 we have:

$$\mu^* = \frac{[34(10^{-1})(T_r^{0.94})]}{\xi} \tag{21}$$

(2.21)

And when T > 1.5 we will have.

$$\mu^* = \frac{[17.78(10^{-1})(4.58T_r - 1.67)^{5/8}]}{\xi} \tag{22}$$

This relationship is suggested for reduced density values ρ_r varying in the interval $0,1 \leq \rho_r < 3$.From the correlation above it is important to observe that the calculated viscosity is given in (micro poise), and that the pressures are provided in atm, and the temperatures in K and densities g/mol [23].

3. Numerical Tools

3.1 Finite Volume Method

In our study, we used the finite volume method, an approach by far the most widely used in the petroleum industry. It offers the advantage of respecting the conditions of mass conservation. Furthermore, it is perfectly suited to the most complex physical problems [31-39].

4. Results and conclusion

4.1. Discussion of results

At a temperature of 600 K, which will be maintained constant, the pressure between the 6 points was calculated, as well as the incoming and outgoing flow rates, as shown in the figures below.

4.2 Calculation of reservoir pressure and flow rate for a critical temperature of 170°C (F0) and an initial pressure of 2700 (psia).

For a reservoir with a pressure of 2700 (psia), which is higher than the critical pressure, the flow rate extracted by the four extraction wells is easier without the intermediate injection well (source) p(n/2,n/2) in the middle of the reservoir, as shown in Figure 3 for the iso-pressure values, and Figure 4 for the outflow rate as a function of pressure. Figure 5 shows the velocity distribution and velocity vector field.

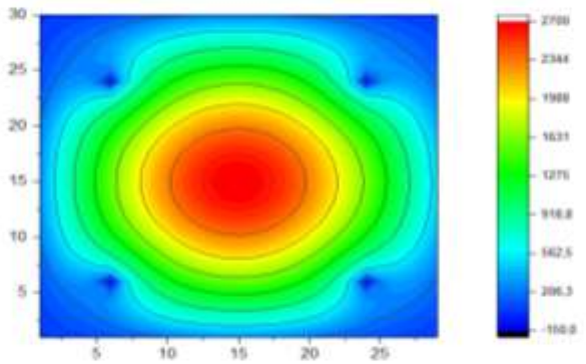

Figure 3. *Pressure curve for a temperature of 170 (F^0) and an initial pressure of 2700 (psia)*

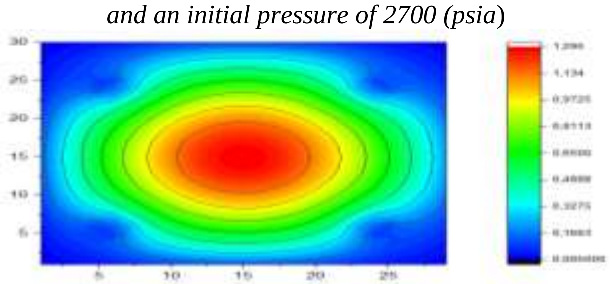

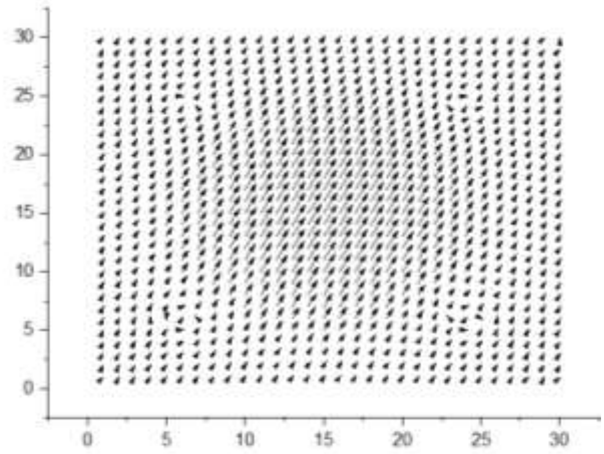

Figure 4. *Velocity curve and velocity vector field of reservoir gas for a temperature of 170 (F^0) and an initial pressure of 2700 (psia)*

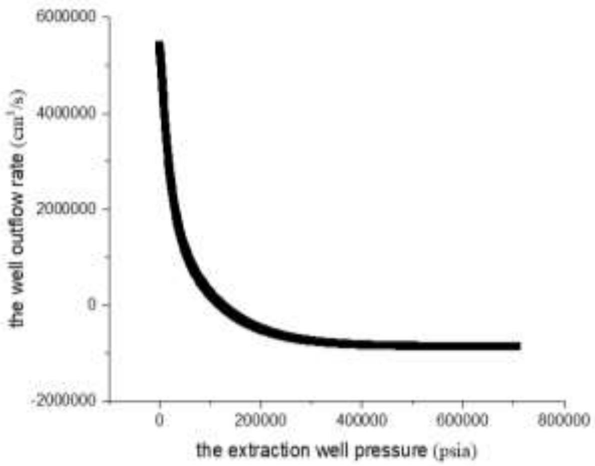

Figure 5. *Gas flow curve for a temperature of 170 (F^0) and an initial pressure of 2700 (psia)*

The pressure distribution shown in Figure 3. shows that the pressure decreases over time from 2700 (psia) to a minimum of 150 (psia). Similarly, the outflow rate in Figure 4. decreases from 6,000,000(cm^3/s) to a minimum flow rate close to 0(cm^3/s). In this case, the pressure should be checked daily to ensure it does not fall significantly below the critical pressure of 2600 (psi).

4.2 Calculation of tank pressure and flow rate for a critical temperature of 170 (F^0) and for an initial pressure of 2600 (psia)

In this case, the pressure increases slightly due to the phase transformation, requiring the addition of capillary pressure terms and saturation terms to the mass transfer equations. Over time, this pressure gradually decreases to 2600 (psi), at which point the CO2 injection well must be used, as shown in Figure 6. Figures 7. and Figures 8. illustrate the velocity distribution, velocity vector field, and gas flow rate in the liquid phase.

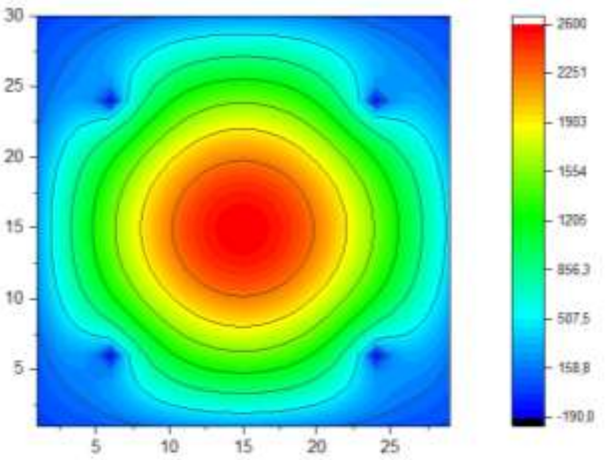

Figure 6. *Pressure curve for a temperature of 170 (F^0) and an initial pressure of 2600 (psia)*

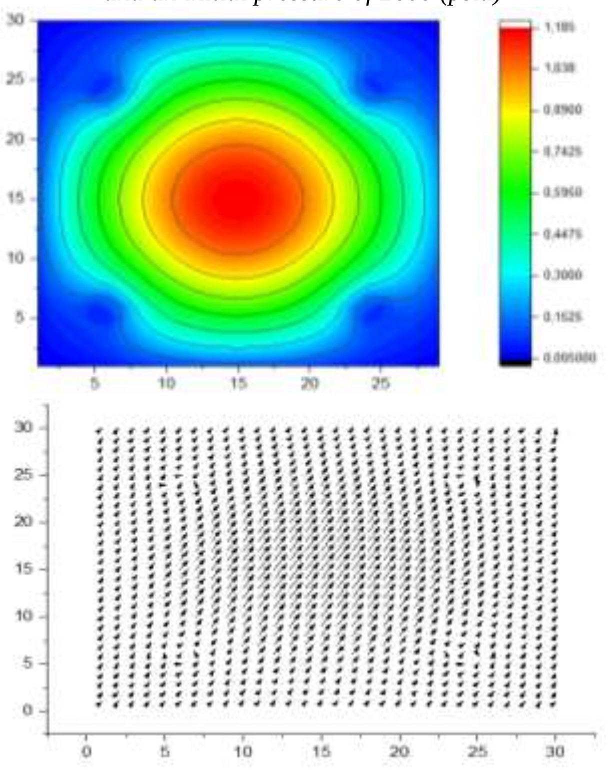

Figure 7. *Velocity curve and velocity vector field of reservoir gas for a temperature of 170 (F^0) and an initial pressure of 2600 (psia)*

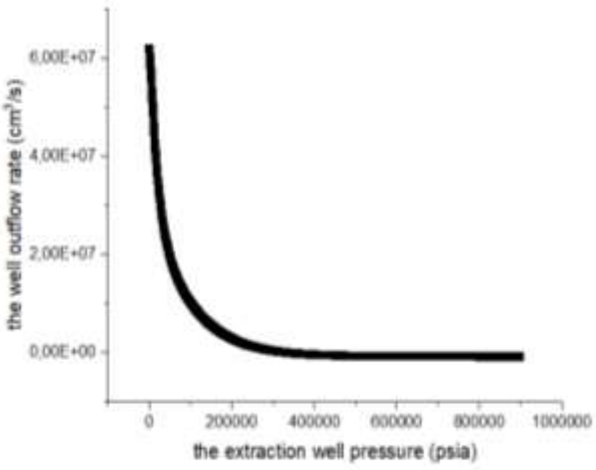

Figure 8. *Gas flow curve for a temperature of 170 (F0) and an initial pressure of 2600 (psia)*

Figure 6. shows that the pressure gradually decreases over time from 2600 (psia) to 158.8(psia). In this case, the fluid, in liquid form, begins to transform into a gas in our extraction wells, and the velocity diffuses to the four extraction wells simultaneously, also decreasing from 1295 (cm^3/s) in the first case to 1180 (cm^3/s) in the second case. Production also decreases from over 6,000,000 (cm^3/s) to 6,000,000 (cm^3/s) in the second case.

4.3 Calculates the pressure and tank flow rate for a critical temperature of 170 (F^0) and for an initial pressure of 2390 (psia).

In this case, we will be in the two-phase (liquid-gas) phase, where we must add the capillary pressure terms and the saturation terms to the mass transfer equations. The reservoir pressure gradually decreases over time until it reaches 2390 (psia), at which point we must use the CO_2 injection well, as shown in Figure 9. Figures 10. and 11. show the distribution, velocity vector field, and gas flow rate exiting in the gaseous phase.

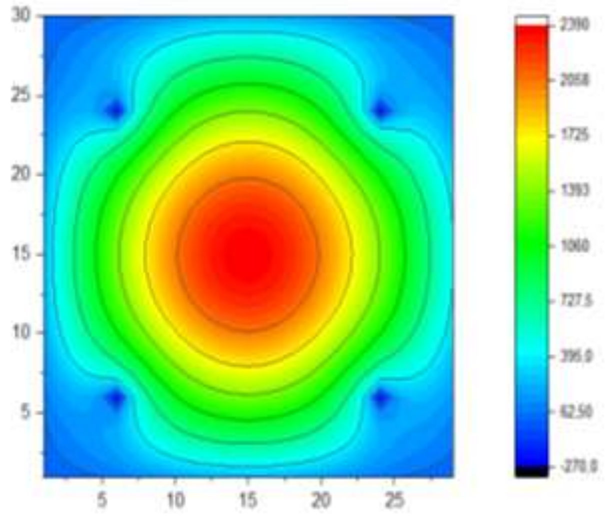

Figure 9. *Pressure curve for a temperature of 170 (F0) and an initial pressure of 2390 (psia).*

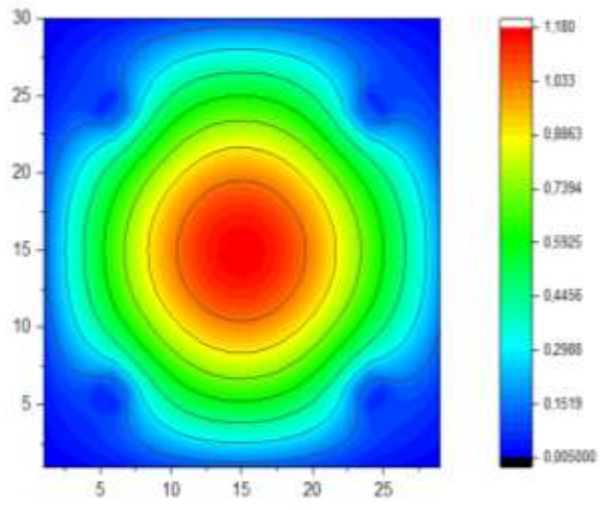

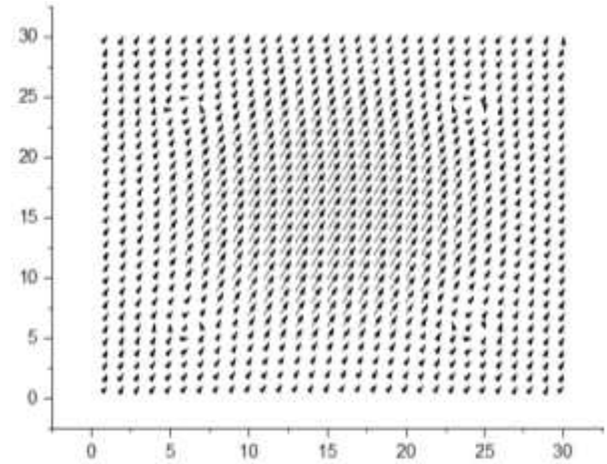

Figure 10. *Velocity curve and velocity vector field of reservoir gas for a temperature of 170 (F0) and an initial pressure of 2390 (psia).*

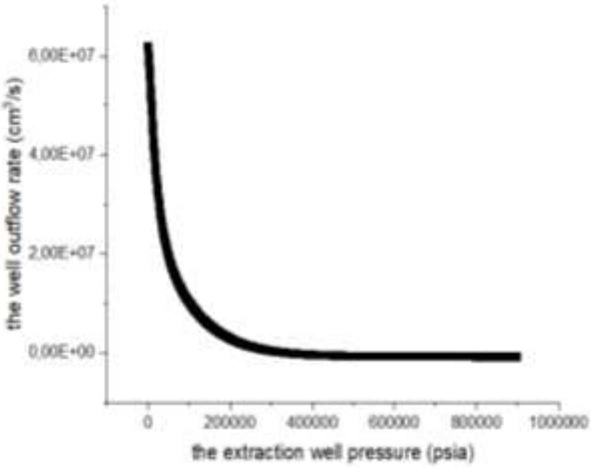

Figure 11. *Gas flow curve for a temperature of 170 (F^0) and an initial pressure of 2390 (psia)*

Figure 9. shows that the pressure gradually decreases over time from 2309 (psia) to 1400 (psia) in the vicinity of the extraction wells. In this case, the fluid, initially a liquid with a velocity varying from 90% to 30%, begins to transform into a gas. Its velocity diffuses simultaneously towards the four extraction wells and also decreases, from 1185 cm^3/s in the second case to 1180 cm^3/s in the third case (Figure 10.). Production also decreases from over 6,000,000 (cm^3/s) to 2,000,000 (cm^3/s) (Figure11).

5. Conclusion

In this study we analyze the behavior of reservoirs in which we try to correctly understand the increase and decrease in fluid production and to carry out the maintenance perspective for these wells, passing through two phenomena: single-phase and two-phase.

In the case where a two-phase fluid is found, there is a pressure increase for a certain time that is not slow enough, so it is necessary to use the injection well to maintain the pressure in the reservoir, as shown in figures 3.4.5.

In the first case, we have the single-phase phenomenon, for which we used a temperature of 170 (F°) and a pressure of 2700 (psia), and we obtained a production of 6,000,000 (cm^3/s). After a certain time, the pressure decreased to 150 (psia), which required us to increase the pressure to 150(psia), with the injection of CO_2 as the injection fluid, to increase the production back to 6,000,000(cm^3/s). But before reaching this stage, we must go through the second case, which is the two-phase phenomenon, where we must check the pressure daily to ensure it does not drop significantly below the critical pressure of 2600(psia). If the pressure decreases to a value of 2309 (psia) and below this value, the fluid will be in a gas-liquid state, or the liquid will vary from 90% to 30%. With the pressure decrease, it is necessary to increase this parameter in the reservoir by injecting CO2 at the injection well. The fluid velocity diffuses towards the 4 extraction wells simultaneously and decreases from 1185 (cm^3/s) in the second case to 1180 (cm^3/s) in the third case. Production also decreases from over 6,000,000(cm^3/s) to 2,000,000 (cm^3/s).

Author Statements:

- **Ethical approval:** The conducted research is not related to either human or animal use.
- **Conflict of interest:** The authors declare that they have no known competing financial interests or personal relationships that could have appeared to influence the work reported in this paper
- **Acknowledgement:** The authors declare that they have nobody or no-company to acknowledge.
- **Author contributions:** The authors declare that they have equal right on this paper.
- **Funding information:** The authors declare that there is no funding to be acknowledged.
- **Data availability statement:** The data that support the findings of this study are available on request from the corresponding author. The data are not publicly available due to privacy or ethical restrictions.

References

[1] Cossé, R. (1988). *Techniques d'exploitation pétrolière: Le gisement* (Vol. 1). Éditions Technip.

[2] Dalvi, S. (2015). Fundamentals of Oil & Gas Industry for Beginners. Notion Press.

[3] Hirsch, M. W., Devaney, R. L., & Smale, S. (1974). *Differential equations, dynamical systems,*

and linear algebra (Vol. 60). Academic press.

[4] Kouadri, A., Benziane, A., Rabehi, A., Rabehi, A., Alhussan, A.A., Khafaga, D.S., El-Kenawy, E.S.M. (2025). A novel hybrid watermarking scheme for medical images using dual-tree complex wavelet and 2D discrete cosine transforms. Traitement du Signal, Vol. 42, No. 5, pp. 2693-2704. https://doi.org/10.18280/ts.420521

[5] Vidal, J. (1997). Thermodynamique: application au génie chimique et à l'industrie pétrolière. Editions Technip.

[6] Tibermacine, I. E., Russo, S., Scarano, G., Tedesco, G., Rabehi, A., Alhussan, A. A., ... & Napoli, C. (2025). Conditional VAE for personalized neurofeedback in cognitive training. PloS one, 20(10), e0335364.

[7] Guermoui, M., Ferkous, K., Rabehi, A., & Belaid, A. (2025). Integrating Hybrid AI Models for Improved PV Power Forecasting: A Path Toward Sustainable Energy. In Artificial Intelligence Applications for a Sustainable Environment (pp. 311-328). Cham: Springer Nature Switzerland.

[8] Teta, A., Elbar, M., Beladel, A., Bakria, D., Korich, B., Chennana, A., & Rabehi, A. (2025). Robust and fast fault diagnosis framework for grid-connected photovoltaic systems via adaptive channel-wise representations and transfer learning. Measurement, 119290.

[9] Mohamed, A., Nacera, Y., Ahcene, B., Teta, A., Belabbaci, E. O., Rabehi, A., ... & Benghanem, M. (2025). Optimized YOLO based model for photovoltaic defect detection in electroluminescence images. Scientific Reports, 15(1), 32955.

[10] Ferkous, K., Menakh, S., Guermoui, M., Bellaour, A., Bekkar, B., Rabehi, A., ... & Benghanem, M. (2025). Optimized solar power forecasting: A multi-decomposition framework using VMD and swarm techniques. AIP Advances, 15(9).

[11] Taibi, A., Ikhlef, N., Aomar, L., Touati, S., Baitiche, O., Alsabah, Y. A., ... & Benghanem, M. (2025). Diagnosis of misalignment faults using the DTCWT-RCMFDE and LSSVM algorithms. Scientific Reports, 15(1), 32128.

[12] Russo, S., Tibermacine, I. E., Randieri, C., Rabehi, A., H Alharbi, A., El-Kenawy, E. S. M., & Napoli, C. (2025). Exploiting facial emotion recognition system for ambient assisted living technologies triggered by interpreting the user's emotional state. Frontiers in Neuroscience, 19, 1622194.

[13] Mostefaoui, M., Kacha, A. H., Rabehi, A., Ameur, K., Mazari, H., & Bluet, J. M. (2025). Study of the effect of the gate’s length on the electrical quality of AlGaN/GaN heterostructures based HEMTs. JOURNAL OF OVONIC RESEARCH, 21(4), 495-504.

[14] Ali, M., Souahlia, A., Rabehi, A., Guermoui, M., Teta, A., Tibermacine, I. E., ... & Benghanem, M. (2025). A robust deep learning approach for photovoltaic power forecasting based on feature selection and variational mode decomposition. Journal of the Nigerian Society of Physical Sciences, 2795-2795.

[15] Ali, M., Rabehi, A., Souahlia, A., Guermoui, M., Teta, A., Tibermacine, I. E., ... & Agajie, T. F. (2025). Enhancing PV power forecasting through feature selection and artificial neural networks: a case study. Scientific Reports, 15(1), 22574.

[16] Atouani, T., Mostefaoui, M., Dennai, B., Rabehi, A., Alsabah, Y. A., & Benghanem, M. (2025). Tension loss analysis at the electrode interface of a dye-sensitized solar cell (DSSC). AIP Advances, 15(7).

[17] Elhannani, A., Brahami, R., Elmeiche, A., Bouamama, M., Rabehi, A., & Benghanem, M. (2025). Analytical Investigation of Free Vibrations in Functionally Graded Material Beams with Different Property Distributions. Nigerian Journal of Technological Development, 22(3), 363-371.

[18] Ghibeche, I., Nourani, A., Naas, T. T., Benziouche, S., Buchholz, M., Buchholz, R., ... & Benghanem, M. (2025). Modeling Climatic Parameters affecting a Greenhouse Irrigation System. Engineering, Technology & Applied Science Research, 15(3), 23352-23359.

[19] Rabehi, A., Meftah, E. H., Benmahmoud, S., Rabehi, A., Alharbi, A. H., & El-kenawy, E. S. M. (2025). SOCA-CFAR Processor in A Homogeneous Erlang-Distributed Clutter: Exact Closed-Form Expression for the Pfa. Traitement du Signal, 42(3).

[20] Ouahabi, M. S., Benyounes, A., Barkat, S., Ihammouchen, S., Rekioua, T., Rabehi, A., ... & Alharbi, A. H. (2025). Real-Time Sensor Fault Tolerant Control of DC-DC Converters in DC Microgrids Using a Switching Unknown Input Observer. IEEE Access.

[21] Tibermacine, I. E., Russo, S., Citeroni, F., Mancini, G., Rabehi, A., Alharbi, A. H., ... & Napoli, C. (2025). Adversarial denoising of EEG signals: a comparative analysis of standard GAN and WGAN-GP approaches. Frontiers in Human Neuroscience, 19, 1583342.

[22] Ladjal, B., Nadour, M., Bechouat, M., Hadroug, N., Sedraoui, M., Rabehi, A., ... & Agajie, T. F. (2025). Hybrid deep learning CNN-LSTM model for forecasting direct normal irradiance: a study on solar potential in Ghardaia, Algeria. Scientific Reports, 15(1), 15404.

[23] Azzazen, M., & Boukraa, S. (2023). Numerical and Experimental Investigation of a Confined Diffusion Flame of Heterogeneous Mixtures. Journal homepage: http://iieta. org/journals/ijht, 41(2), 415-422.

[24] Mehallel, E., Bouchemel, A., & Rebahi, A. (2025). A Fast Enhanced Medical Image Encryption scheme Based on 2D-Chaotic Map and Improved Zigzag confusion. ITEGAM-JETIA, 11(52), 205-219.

[25] Bendelala, F., Bellakhdar, A., Baitiche, O., Cheknane, A., Helal, M. H., Hilal, H. S., & Rabehi, A. (2025). FDTD Modelling of Nanostructured Hemispherical Plasmonic Light Trapping for Enhanced Ultra-thin GaSb TPV

Cell. Semiconductors, 59(4), 404-411.
[26] Khelifi, R., Chekifi, T., Belaid, A., Guermoui, M., Rabehi, A., Khaled, F., ... & Agajie, T. F. (2025). Comparative performance analysis of hemispherical solar stills using date and olive kernels as heat storage material. Scientific Reports, 15(1), 7128
[27] Chennana, A., Megherbi, A. C., Bessous, N., Sbaa, S., Teta, A., Belabbaci, E. O., ... & Agajie, T. F. (2025). Vibration signal analysis for rolling bearings faults diagnosis based on deep-shallow features fusion. Scientific Reports, 15(1), 9270.
[28] Bentegri, H., Rabehi, M., Kherfane, S., Nahool, T. A., Rabehi, A., Guermoui, M., ... & El-Kenawy, E. S. M. (2025). Assessment of compressive strength of eco-concrete reinforced using machine learning tools. Scientific Reports, 15(1), 5017.
[29] Mehallou, A., M'hamdi, B., Amari, A., Teguar, M., Rabehi, A., Guermoui, M., ... & Khafaga, D. S. (2025). Optimal multiobjective design of an autonomous hybrid renewable energy system in the Adrar Region, Algeria. Scientific Reports, 15(1), 4173.
[30] Boukredine, S., Mehallel, E., Boualleg, A., Baitiche, O., Rabehi, A., Guermoui, M., ... & Tibermacine, I. E. (2025). Enhanced Performance of Microstrip Antenna Arrays through Concave Modifications and Cut-Corner Techniques. ITEGAM-JETIA, 11(51), 65-71.
[31] Belaid, A., Guermoui, M., Riche, A., Arrif, T., Maamar, Rabehi, A., C. M., ... & Al Rahhal, M. M. (2024). High-Resolution Mapping of Concentrated Solar Power Site Suitability in Ghardaïa, Algeria: A GIS-Based Fuzzy Logic and Multi-Criteria Decision Analysis. IEEE Access.
[32] Younsi, A. M., Elbar, M., & Rabehi, A. (2024). Structural, Electronic, and Optical Properties of Perovskites CaATe3 (A= Zr Or Hf): A Theoretical Investigation. Semiconductors, 58(12), 984-992.
[33] Daha, R., Bouloudenine, M., Khiat, A., Gomez, C. V., La Pietra, M., Rabehi, A. E., ... & Bellucci, S. (2024). Enhancement of Cobalt Ferrite Properties through Rare Earth Ion Doping. Semiconductors, 58(12), 993-1005.
[34] Belaid, A., Guermoui, M., Khelifi, R., Arrif, T., Chekifi, T., Rabehi, A., ... & Alhussan, A. A. (2024). Assessing Suitable Areas for PV Power Installation in Remote Agricultural Regions. Energies, 17(22), 5792.
[35] Marzouglal, M., Souahlia, A., Bessissa, L., Mahi, D., Rabehi, A., Alharthi, Y. Z., ... & Ghoneim, S. S. (2024). Prediction of power conversion efficiency parameter of inverted organic solar cells using artificial intelligence techniques. Scientific Reports, 14(1), 25931.
[36] Ziane, A., Rabehi, A., Rouabhia, A., Amrani, M., Douara, A., Dabou, R., ... & Sahouane, N. (2024). Numerical Investigation of G–V Measurements of metal–A Nitride GaAs junction. Revista Mexicana de Física, 70(6 Nov-Dec), 061604-1.
[37] Mekaret, F., Rabehi, A., Zebentout, B., Tizi, S., Douara, A., Bellucci, S., ... & Alhussan, A. A. (2024). A comparative study of Schottky barrier heights and charge transport mechanisms in 3C, 4H, and 6H silicon carbide polytypes. AIP Advances, 14(11).
[38] Douara, A., Rabehi, A., Guermoui, M., Daha, R., & Tibermacine, I. E. (2024). Simulation-based optimization of barrier and spacer layers in InAlN/GaN HEMTs for improved 2DEG density. Micro and Nanostructures, 195, 207950.
[39] Rabehi, A., Douara, A., Mohamed, E., Zenzen, R., & Amrani, M. (2024). Impact of Grain Boundaries on The Electrical Characteristics and Breakdown Behavior of Polycrystalline Silicon Pin Diodes: A Simulation Study. ITEGAM-JETIA, 10(49), 59-64.